ACS Biomaterials SCIENCE & ENGINEERING

Article

Cite This: ACS Biomater. Sci. Eng. 2018, 4, 90–97

Inhibition of Bacterial Adhesion on Nanotextured Stainless Steel 316L by Electrochemical Etching

Yeongseon Jang,[†,⊥] Won Tae Choi,[†,‡,⊥] Christopher T. Johnson,[§] Andrés J. García,[∥] Preet M. Singh,[‡] Victor Breedveld,[†] Dennis W. Hess,[*,†] and Julie A. Champion[*,†]

[†]School of Chemical and Biomolecular Engineering, Georgia Institute of Technology, 311 Ferst Drive, Atlanta, Georgia 30332, United States

[‡]School of Material Science and Engineering, Georgia Institute of Technology, 500 10th Street, Northwest, Atlanta, Georgia 30332, United States

[§]Coulter Department of Biomedical Engineering, Georgia Institute of Technology and Emory University, Atlanta, Georgia 30332, United States

[∥]Woodruff School of Mechanical Engineering, Petit Institute for Bioengineering and Bioscience, Georgia Institute of Technology, 315 Ferst Drive, Atlanta, Georgia 30332, United States

Supporting Information

ABSTRACT: Bacterial adhesion to stainless steel 316L (SS316L), which is an alloy typically used in many medical devices and food processing equipment, can cause serious infections along with substantial healthcare costs. This work demonstrates that nanotextured SS316L surfaces produced by electrochemical etching effectively inhibit bacterial adhesion of both Gram-negative *Escherichia coli* and Gram-positive *Staphylococcus aureus*, but exhibit cytocompatibility and no toxicity toward mammalian cells in vitro. Additionally, the electrochemical surface modification on SS316L results in formation of superior passive layer at the surface, improving corrosion resistance. The nanotextured SS316L offers significant potential for medical applications based on the surface structure-induced reduction of bacterial adhesion without use of antibiotic or chemical modifications while providing cytocompatibility and corrosion resistance in physiological conditions.

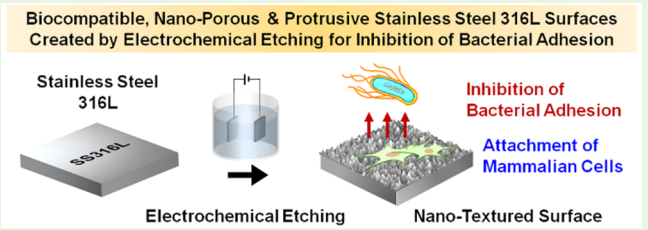

KEYWORDS: *stainless steel 316L, nanostructure, bacterial adhesion, fibroblast, biomedical applications*

INTRODUCTION

Bacterial adhesion and growth on surfaces of medical devices lead to serious surgical and implant infection problems which can be life-threatening and incur substantial healthcare costs.[1] From many previous studies on the interaction between bacteria and surfaces, it is believed that the initial bacterial adhesion steps prior to the formation of extracellular polymeric substances are mediated by long-range nonspecific interactions such as hydrodynamic, hydrophobic, van der Waals, and electrostatic interactions.[2,3] In the bacterial adhesion process, physicochemical surface characteristics dominantly impact the interfacial rearrangement of cells to maximize adhesion to surfaces via nonspecific or ligand-specific interactions.[4]

To develop functional surfaces inhibiting bacterial adhesion, chemical coatings of either antimicrobial agents such as silver,[5] copper, or quaternary ammonium compounds[6] or antifouling polymers such as polyethylene glycol,[7] poly(*N*-isopropylacrylamide),[8] or zwitterionic polymer[9] have been applied. However, considerable drawbacks to such approaches exist, including the possibility of drug resistance, toxicity to mammalian cells, delamination, and functionality loss when coating agents are exhausted due to hydrolytic or thermal degradation.[10,11] In addition, antiadhesive coatings can provide nonspecific resistance to adhesion of bacteria, proteins, viruses, and mammalian cells, thus interfering with desirable interactions.

Recently, another strategy to generate antibacterial surfaces has been considered through the use of nanotechnology. Advances in nanofabrication techniques have led to the development of nanostructured surfaces on diverse materials for antibacterial properties. For example, gold or nickel nanomaterials deposited on metals,[12,13] nanoimprinted polymers,[14,15] and porous alumina surfaces[16] all exhibited reduced bacterial adhesion. Feng et al. demonstrated that the reduction of bacterial adhesion originates from electrostatic repulsion between bacteria and nanoporous surfaces.[17] In addition, nanoprotrusions were fabricated on silicon surfaces by mimicking insect wings that display bactericidal effects.[18] However, questions remain, including whether nanostructures on other material surfaces will also inhibit bacterial adhesion, and which nanofabrication methods and materials are most

Received: August 2, 2017
Accepted: November 28, 2017
Published: December 12, 2017

DOI: 10.1021/acsbiomaterials.7b00544
ACS Biomater. Sci. Eng. 2018, 4, 90–97

appropriate for practical use. Additional challenges are to make surfaces compatible with mammalian cell adhesion for tissue integration and to develop methods to generate nanostructures on current biomedical device surfaces while maintaining their original material properties.

Stainless steel 316L (SS316L) is commonly used in biomedical applications such as surgical tools and cardiovascular and orthopedic implants due to its adequate mechanical strength, corrosion resistance, and biocompatibility.[19] Nonetheless, there have been few studies on the effect of SS surface topography on the bacterial adhesion, and most work has focused on surface roughness at the tens of nanometers to micrometer scale. To the best of our knowledge, there are only two reports of surface-roughened SS316L that study the effect on bacterial adhesion. They utilize severe shot peening (SSP)[20] and magneto rheological abrasive flow finishing (MRAFF),[21] which control SS316L roughness in the range of 10 to 40 nm. The shot-peened SS316L surfaces exhibited a reduction in adhesion of Gram-positive bacteria, *Staphylococcus aureus* (*S. aureus*) and *Staphylococcus epidermidis* (*S. epidermidis*), which account for two-thirds of orthopedic implant infections, with an increase in surface roughness.[20] While the SSP-treated SS316L surfaces had no impact on Gram-negative *Escherichia coli* (*E. coli*) adhesion, the MRAFF-treated SS316L surfaces showed an increase in *E. coli* adhesion as surface roughness increased.[21] In the cases of other surface types with similar surface roughness parameters, nanotextured polymer surfaces with root mean square (RMS) roughness of 13.8 nm successfully inhibited *S. aureus* growth but had much less influence on *E. coli* adhesion,[14] while the adhesion of *E. coli* and *S. aureus* were enhanced as the RMS surface roughness of titania thin films increased up to about 20 nm.[22] These results indicate that adhesion and growth of bacteria are strongly dependent on the surface types, the bacterial species, and the surface finishing methods that dictate the surface topography and chemistry.

Gram-negative bacteria have a unique outer membrane surrounding peptidoglycan layer, which accounts for more antibiotic resistance.[23] The more fluidic outer membrane of Gram-negative bacteria, as compared with the rigid peptidoglycan layer of Gram-positive bacteria, may interact differently with nanotextured surfaces.[14,20] Since current understanding of the effect of nanotextured surfaces on initial bacterial adhesion is very limited, more studies using different cell strains and surface materials are necessarily required. Also, considering that fast evolution of *E. coli* with increasing drug resistance is a growing problem,[24,25] there is a significant need to develop effective antibacterial surfaces for both Gram-positive and Gram-negative bacteria. Therefore, the aim of this work is to evaluate the in vitro antibacterial nature of nanotextured SS316L surfaces created by electrochemical etching, which possess pronounced nanoporous and protrusive structures on the surface.[26] Compared to other surface finishing techniques, the electrochemical etching process is affordable, fairly scalable, and has fine control of surface structures by electrochemical parameters such as potential and current density.[26] Furthermore, electrochemically etched SS316L surfaces form a superior passive layer for corrosion resistance,[27] which would be another advantage to use this method for biomedical applications.

EXPERIMENTAL SECTION

Materials. Nitric acid (ACS reagent, 70%) and SS316L plates (30 × 20 × 0.05 cm^3) were purchased from Sigma-Aldrich and Maudlin Products, respectively. Insulating tape (electroplating tape 470) was purchased from 3M. Organic solvents acetone (99.5%), methanol (99.8%), and isopropanol (99.5%) were purchased from VWR International.

SS316L Sample Preparation. Two different sizes (2.5 × 1.5 × 0.05 and 2.5 × 2.5 × 0.05 cm^3) of SS316L samples were prepared by using a water jet cutter. These two SS316L samples served as working and counter electrodes, respectively. Prior to electrochemical surface modification, the samples were rinsed with acetone, methanol, and isopropanol to remove organic contaminants and subsequently air-dried at ambient temperature. Electrical connections of SS wire onto the SS316L samples were established by spot-welding. The working electrode was masked with insulating tape, leaving an active area of 0.19 cm^2 for electrochemical surface modification. Diluted nitric acid solution (48% by weight) was used as the electrolyte. A three-electrode system was used with a saturated calomel electrode (SCE) serving as the reference electrode. The separation distance between working and counter electrodes was maintained at 3 cm. A potentiostat (Gamry Reference 600) was used to perform electrochemical surface modification. After initial delays of 60 s at open circuit conditions, potentiostatic polarizations were conducted at anodic potentials of 2.2 V (vs SCE) for 60 s at room temperature, which generated nanotextured (NT)-SS316L surfaces. The anodic potential value, 2.2 V (vs SCE), was chosen based on our previous study showing the relationship between applied anodic potential and surface topography of the electrochemically etched stainless steel 316L.[26] After potentiostatic electrochemical surface modification, the SS316L samples were removed from the electrochemical cell, washed with deionized water, and dried at room temperature for one day prior to characterization.

SS316L Surface Characterization. Surface morphologies of SS316L samples were characterized by scanning electron microscopy (SEM, Hitach SEM SU8010) at 3 kV acceleration potential, and topographical information was acquired by atomic force microscopy (AFM, Veeco Dimension 3100) using AppNano ACT tapping mode AFM probes (Applied Nanosciences). The surface roughness parameters of AR-SS316L and NT-SS316L surfaces were obtained by AFM measurements from scanning a surface area of 4 μm^2 while avoiding artificial defect areas. The quantitative data of the mean roughness (R_a) and the root-mean-square (RMS) roughness (R_q) were analyzed by image processing with the Gwyddion program. Chemical composition of SS316L surfaces were analyzed by X-ray photoelectron spectroscopy (XPS, Thermo Fisher Scientific K-Alpha XPS) with a 400 μm microfocused monochormatic Al Kα X-ray source, which has analysis depth of less than 5 nm.

Corrosion Test. Corrosion behavior of SS316L samples was tested by potentiodynamic polarization in Hank's balanced salt solution (Gibco). The as-received and nanotextured SS316L samples with exposed area of 0.19 cm^2 were used as working electrodes. SCE and platinum foil were used as reference and counter electrodes, respectively. After an initial delay of 1800 s at open circuit conditions, the SS316L samples were polarized to the anodic direction from −0.05 V (vs open circuit potential) to 1.0 V (vs SCE) with a scan rate of 0.2 mV/s. During the polarizations, the scans were stopped when the SS316L samples showed localized corrosion, indicated by a sudden increase in current density by more than two orders of magnitude. Gamry EChem Analyst software was used to perform Tafel fitting on the potentiodynamic polarization curves. All corrosion tests were performed at room temperature.

Bacterial Cultures and Assays. Gram-negative *E. coli* (BL21)[28] and Gram-positive *S. aureus* (ATCC49230)[29] were used in this study as model microorganisms for bacterial adhesion assays. The SS316L samples sterilized by autoclave (15 psi, 121 °C for 20 min) were transferred into 6-well cell culture plates and incubated with 5 mL of bacterial solution with optical density 0.3 (≈ 5 × 10^7 cells/mL) in lysogency broth (LB) media for *E. coli* or in tryptic soy broth (TSB) media for *S. aureus*. Bacteria were cultured on the samples for 24 and 48 h in an static incubator (37 °C, humidified air). The medium was exchanged with 5 mL of sterile fresh LB media after 24 h. To quantify the number of *E. coli* and *S. aureus* adhered to each SS316L surface, the

DOI: 10.1021/acsbiomaterials.7b00544
ACS Biomater. Sci. Eng. 2018, 4, 90−97

colony forming units (CFUs) of adhered cells were counted using the spread plate method.[30] At the end of incubation, samples were rinsed three times with phosphate-buffered saline (PBS) and transferred into a 50 mL tube with 5 mL of fresh PBS. Each sample was sonicated for 7 min and vortexed for 20 s to release bacteria remaining on the sample surface into the solution. The initial dilution was made by transferring 25 μL of the resuspended cell solution into 225 μL of fresh PBS (10^{-1} dilution), and a series of diluted solutions ($10^{-1} \sim 10^{-8}$) in PBS was prepared in 96-well plates. Then, 0.1 mL of each diluted solution of *E. coli* and *S. aureus* was spread onto LB or tryptic soy agar plates (i.e., 0.1 mL/agar), respectively. Bacterial colonies, between 30 and 300 colonies on each plate, were counted after 24 h of incubation at 37 °C. The number of bacteria (CFU) per sample was calculated by dividing the number of colonies by the dilution factor multiplied by the amount of cell suspension plated to agar (0.1 mL), then multiplying by the initial volume of cell suspension (5 mL).

To visualize bacterial adhesion on the surface using SEM, SS316L samples were prepared and incubated in bacterial solution with the same procedure described above. After incubation, SS316L samples were gently washed with PBS three times, fixed with 2.5% glutaraldehyde solution for 1 h, and then dehydrated using a series of ethanol concentrations in distilled water (i.e., 50, 70, 90, and 100% ethanol for 20 min). The dehydrated samples were dried by hexamethyldisilazane (HMDS, Aldrich) treatments overnight and then sputter coated with gold (~7 nm) with a Quorum Q-150T ES Sputter Coater prior to SEM analysis. Surface morphologies of the SS316L samples were characterized by SEM (Hitach SEM SU8010) at 3 kV acceleration potential.

Confocal Laser Scanning Microscopy for Bacterial Viability Assay. To characterize both cell viability and adhesion in the early stage of interaction, the AR-SS316L and NT-SS316L samples were incubated in *E. coli* solution with a cell density of ~10^8 cells/mL for 30 min in a static incubator (37 °C, humidified air). Then, the samples were washed with PBS and stained with the Live/Dead BacLight bacterial viability kit (Life Technologies) for fluorescence microscopy analysis. Equal volumes of 3.34 mM SYTO9 (green dye for live cells) and 20 mM propidium iodide (red dye for dead cells) were mixed together in 1 mL of PBS. The staining solution was added onto each sample and allowed to incubate in the dark for 15 min. Then, the samples were flipped upside down into a slide glass and imaged under a 20× objective using a Nikon-C2 laser scanning confocal microscope. Live bacteria were imaged using a 488 nm laser with a 525/50 nm filter and dead bacteria with a 561 nm laser with a 595/50 nm filter.

Fibroblast Cell Cultures and Assays. NIH-3T3 mouse fibroblast cells (CRL-1658, ATCC) were cultured in Dulbecco's modified Eagle's medium (DMEM, ATCC) supplemented with 10% fetal bovine serum (FBS, Sigma-Aldrich) and 1% penicillin/streptomycin (P/S, Gibco). The cleaned and sterilized SS316L samples were placed individually into the wells of a 24-well plate. The cells were seeded onto the samples at a density of 10 000 cells/mL per substrate and placed in an incubator for 24, 72, and 96 h at 37 °C with a humidified 5% CO_2 atmosphere. Cell metabolic activity was determined using a quantitative colorimetric conversion assay of 3-[4,5-dimethylthiazol-2-yl]-2, 5-diphenyl tetrazolium bromide (MTT). Cells on polystyrene tissue culture control dish, AR- and NT-SS316L surfaces were incubated with MTT solution for 3 h and washed with PBS. The formazan product was solubilized in dimethyl sulfoxide (DMSO), and the reacted solutions only transferred for reading absorbance at 570 and 630 nm as determined with a microplate reader (Bio-TEK Instruments, INC). We compared cytocompatibility between samples by normalization of the averaged cell metabolic activity in control dishes to 100%.

The morphology of NIH-3T3 cells adhered on the SS316L surfaces was investigated by SEM after 24 h of incubation. After PBS washing, the samples were fixed with 4% paraformaldehyde for 4 h at 4 °C, then dehydrated and dried using a series of ethanol concentrations and HMDS in the same way as the bacterial SEM samples. Fibroblast adhered SS316L samples were also sputter coated with gold (~7 nm) using Quorum Q-150T ES Sputter Coater prior to SEM analysis. Surface morphologies of the SS316L samples were characterized by SEM (Hitach SEM SU8010) at 3 kV acceleration potential.

Statistical Analysis. All experiments for bacterial and mammalian cell studies were performed in triplicate. Mean values with the standard error of the mean (mean ± SEM) were calculated, and the statistical significance was assessed with *t*-test with *p*-values less than 0.05 considered to be significant.

RESULTS AND DISCUSSION

We prepared as-received and nanotextured stainless steel 316L (AR-SS316L and NT-SS316L) samples (Figure 1). The NT-SS316L surface was produced by electrochemical etching at an anodic potential of 2.2 V (vs SCE) (Figure 1a). The AR-SS316L represents a commercially available SS316L substrate serving as a control. Three dimensional topography profiles and surface morphologies of SS316L samples were obtained by AFM and SEM, respectively (Figures 1b and c). The AR-SS316L displays typical defects and micrometer-scale surface features created during the manufacturing process. The NT-SS316L surface exhibits nanopores with pore diameters of 20–25 nm and sharp nanoprotrusions.

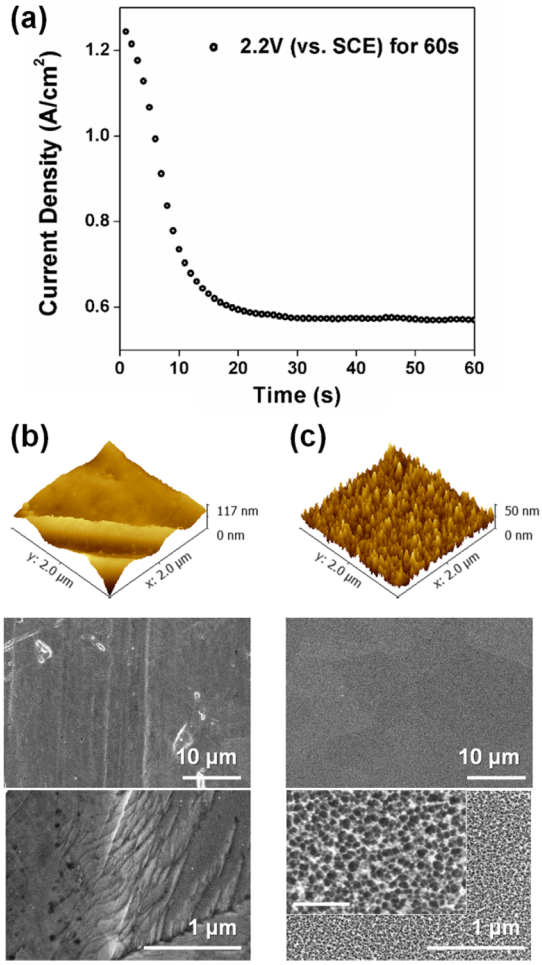

Figure 1. Structure characterization of stainless steel 316L surfaces after electrochemical modification. (a) Potentiostatic polarization at an anodic potential of 2.2 V (vs a saturated calomel electrode (SCE)) for fabricating a nanotextured SS316L (NT-SS316L) surface. Three dimensional AFM topography profiles and SEM images of (b) as-received (AR-SS316L) and (c) nanotextured (NT-SS316L) surfaces. The scale bar of the inset SEM image is 200 nm.

DOI: 10.1021/acsbiomaterials.7b00544
ACS Biomater. Sci. Eng. 2018, 4, 90–97

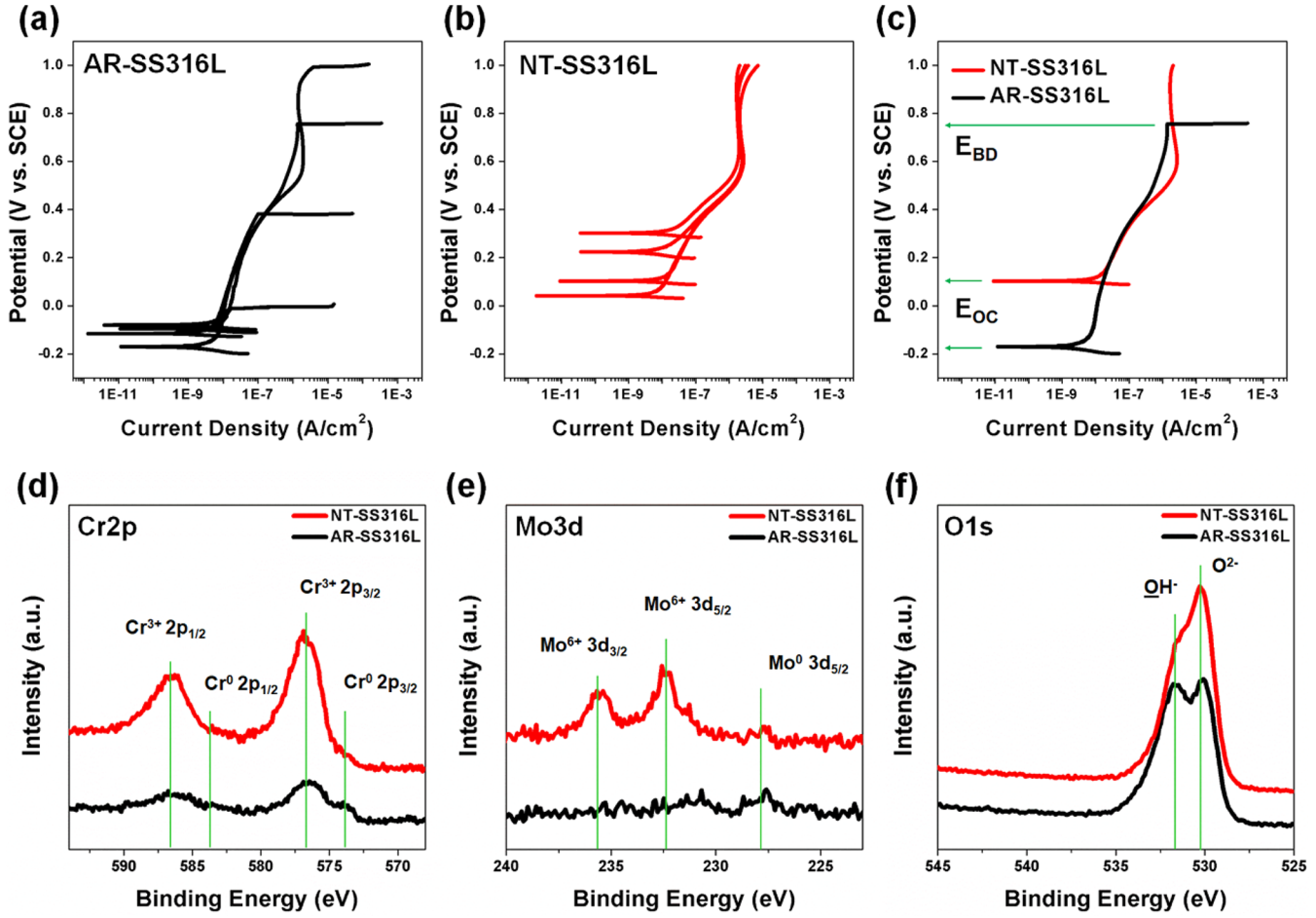

Figure 2. Corrosion behavior of SS316L samples in Hank's balanced salt solution and chemical composition of SS316L surfaces. Potentiodynamic polarization curves of (a) AR- and (b) NT-SS316L samples and (c) representative curves for each SS316L sample. XPS spectra of (d) Cr 2p scans, (e) Mo 3d scans, and (f) O 1s scans of AR- and NT-SS316L surfaces.

Previous studies estimated surface−bacteria interaction forces using the extended Derjaguin−Landau−Verwey−Overbeek (DLVO) theory and demonstrated that the reduction of bacterial adhesion of the nanoporous surface originates from synergetic repulsion due to electrostatic and acid−base repulsive forces and effective surface free energy.[16,17] On the basis of the calculations, the authors found that the most effective pore diameter for inhibiting bacterial adhesion is 15 to 25 nm, which is in a good agreement with their experimental results using nanoporous anodized aluminum oxide surfaces.[17] Surface roughness is also an important parameter affecting bacterial adhesion behavior. The AR-SS316L and NT-SS316L surfaces presented arithmetic mean roughness (R_a) of 1.683 and 5.184 nm and RMS roughness (R_q) of 2.131 and 6.509 nm, respectively (Figure S1 in Supporting Information). Most previous work reported that nanotextured surfaces effectively inhibit bacterial adhesion as compared with nontextured surfaces, but the range of roughness parameters that reduce bacterial adhesion varied widely with the surface types,[14,22] the surface modification methods applied,[20,21,31] the roughness parameters determined, the method used to detect the bacteria on surfaces, and the bacterial species studied.[32] In addition, surface nanoprotrusions display a bactericidal effect, which is attributed to mechanical stress exerted on the membrane of bacteria adhered to the nanoprotrusions, resulting in bacterial membrane stretching, rupture and death.[33] The beneficial combination of desired pore size and surface nanospikes suggest that the NT-SS316L sample will effectively inhibit adhesion of both Gram-positive and Gram-negative bacteria.[20]

For biomedical applications, corrosion resistance is an essential characteristic. In particular, cells and their metabolic products on SS316L surface in physiological solutions often induce and accelerate localized corrosion such as pitting and crevice corrosion at the surface.[34,35] The localized corrosion attacks can become an initiation site for mechanical failure of SS316L implants, and the released metal ions during localized corrosion can cause inflammation of surrounding tissues.[34] Hence, improving localized corrosion resistance of SS316L surfaces in physiological solutions is significant when considering their uses in biomedical applications.

We conducted potentiodynamic polarizations for AR- and NT-SS316L in Hank's balanced salt solution to determine corrosion resistance under physiological conditions. Due to the stochastic behavior of localized corrosion,[36,37] four samples for each SS316L surface were tested (Figures 2a and b), and each representative potentiodynamic polarization curve was selected for comparison (Figure 2c). The AR- and NT-SS316L samples were polarized from −0.05 V (vs open circuit potential, E_{OC}) to anodic direction up to 1.0 V (vs SCE), and corrosion tests were stopped when localized corrosion occurred, which is identified by a sharp increase in current density. The potential at this point is denoted as breakdown potential (E_{BD}) (Figure 2c).[38]

DOI: 10.1021/acsbiomaterials.7b00544
ACS Biomater. Sci. Eng. 2018, 4, 90−97

While AR-SS316L samples exhibited localized corrosion with E_{BD} of 0.53 ± 0.44 V (vs SCE), local breakdowns were not observed on NT-SS316L samples up to the anodic polarization of 1.0 V (vs SCE). This result demonstrates superior localized corrosion resistance of NT-SS316L compared to AR-SS316L surfaces. In addition, Tafel fittings were performed to the potentiodynamic polarization curves to obtain corrosion potentials (E_{corr}) and corrosion current densities (I_{corr}) of AR- and NT-SS316L samples in Hank's balanced salt solution (Figure S2 in the Supporting Information, Table 1). The E_{corr} of NT-SS316L was ~0.3 V more anodic (noble) than that of AR-SS316L, implying less corrosion susceptibility. Slightly increased I_{corr} of NT-SS316L compared to AR-SS316L is attributed to increase in surface area of NT-SS316L. Electrochemical etching provides significant benefit of improving corrosion resistance in addition to the development of pronounced nanotextures on the surface.

Table 1. Corrosion Behavior of AR- and NT-SS316L in Hank's Balanced Salt Solution

	AR-SS316L	NT-SS316L
E_{corr} (V vs SCE)	−0.13 ± 0.04	0.17 ± 0.12
I_{corr} (μA/cm^2)	0.007 ± 0.003	0.013 ± 0.005
E_{BD} (V vs SCE)	0.53 ± 0.44	

Because corrosion behavior is largely affected by chemical composition of the SS316L surface, XPS was performed for AR- and NT-SS316L samples (Figures 2d–f). XPS spectra of Cr 2p and Mo 3d confirm the increases in Cr and Mo content on the NT-SS316L surface compared to that on the AR-SS316L surface. O 1s XPS spectra indicate that the NT-SS316L samples have more oxide than hydroxide content. Chromium oxide (Cr_2O_3) is the primary contributor to corrosion resistance of stainless steels, while the Mo content at the surface stabilizes the Cr_2O_3 passive layer.[39] Therefore, the superior corrosion resistance of NT-SS316L surface is attributed to the formation of beneficial surface chemistry after the electrochemical surface modification. Furthermore, it is notable that the AR- and NT-SS316L surfaces present similar water wettability (Figure S3 in Supporting Information), which implies that surface hydrophobicity does not play a significant role in this case.

To assess the efficiency of NT-SS316L surfaces in reducing bacterial adhesion as compared with AR-SS316L surfaces, we monitored the adhesion and growth of Gram-positive *S. aureus* and Gram-negative *E. coli* by colony forming unit (CFU) counting and SEM (Figure 3). Number of adherent bacteria on the AR- and NT-SS316L surfaces was evaluated by counting CFU, which indicates adhered and viable bacteria on that surface, following bacterial culture for 24 and 48 h. The quantity of *S. aureus* adhered on NT-SS316L surfaces was 86.2 and 81.2% less than on AR-SS316L surfaces after 24 and 48 h culture, respectively (Figure 3a). It is clear that adhesion and/or growth of *S. aureus* was effectively prevented on the NT-SS316L surfaces as compared with the AR-SS316L surfaces.

Importantly, the same effect of NT-SS316L surfaces on bacterial adhesion was also observed for Gram-negative *E. coli*. Previous studies showed that Gram-negative *E. coli* was much less susceptible to surface nanotextures than Gram-positive *S. aureus*.[14,20] These results may be attributed to less pronounced nanoscale surface roughness and the distinctive membrane features of Gram-negative bacteria. A significant increase in *E. coli* adhesion was measured on the AR-SS316L surface from 24 to 48 h, whereas *E. coli* growth and/or attachment was inhibited on the NT-SS316L surfaces 95.9 and 99.6%, respectively (Figure 3b). This antibacterial adhesion effect of the NT-SS316L surfaces may be attributed to the precisely controlled nanopores with diameters of about 20 nm along with their sharp edges, resulting in the membrane stress required to

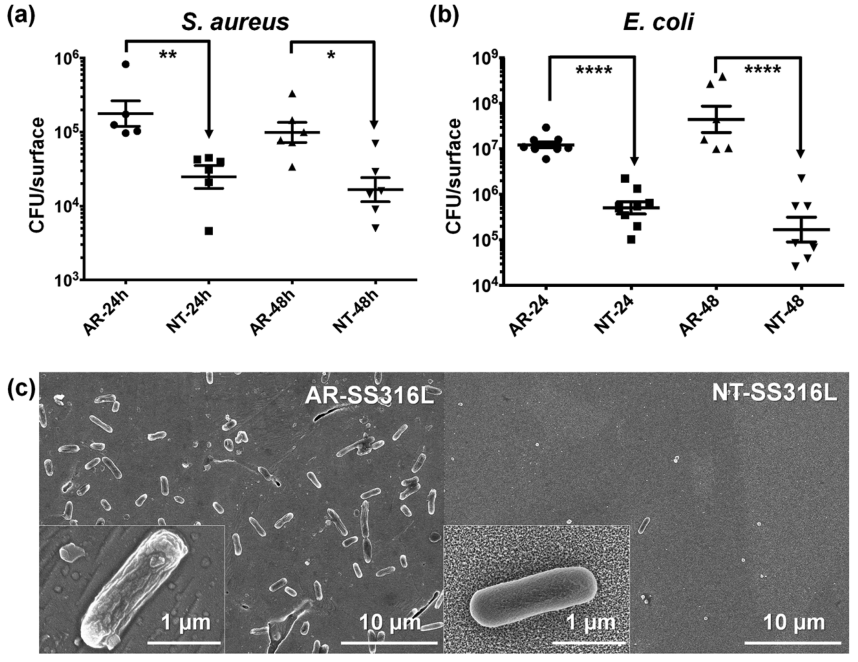

Figure 3. Bacterial adhesion on SS316L surfaces. Number of adhered (a) *S. aureus* and (b) *E. coli* cells on AR- (●) and NT- (■) SS316L surfaces following 24 and 48 h of incubation (data represent mean ± SEM, $N = 3$). The quantity of adhered cell number was characterized by counting CFU per sample (* $p < 0.05$, ** $p < 0.005$, **** $p < 0.0001$ compared with AR-SS316L samples at the same time period). (c) SEM images show the number and morphology of *E. coli* adhered on AR- (left) and NT-SS316L (right) surfaces after 24 h of culture.

DOI: 10.1021/acsbiomaterials.7b00544
ACS Biomater. Sci. Eng. 2018, 4, 90–97

stretch between the nanopillars and nanopores.[14−18] Furthermore, *E. coli* cells growing on AR-SS316L present a rumpled, wrinkled morphology, which indicates strong adhesion of *E. coli* to an abiotic surface with the formation of fimbriae.[40] On the other hand, *E. coli* adhered on the NT-SS316L surface do not exhibit morphological changes, thereby suggesting a weaker adhesion on the NT surface (Figure 3c).

The surface roughness on SS316L can be controlled by tuning electrochemical etching parameters. In our previous work,[26] we controlled the electrochemical etching parameters, including anodic potential, to vary surface roughness on SS316L. As a result, we confirmed that the low applied anodic potential (1.1−1.6 V vs SCE) resulted in micrometer scale surface roughness, while the higher anodic potential (1.8−2.2 V vs SCE) yielded a nanotextured (NT) surface. We tested *E. coli* adhesion for 24 h on microscale roughness imparted SS316L, but there was no significant reduction in bacterial adhesion on the microtextured SS316L compared to that of AR-SS316L (Figure S4 in Supporting Information). Hence, we focused on the NT-SS316L in this study.

We performed Live/Dead fluorescent microscopy assays to investigate if the bacteria are killed by nanoprotrusive characteristics of the NT-SS316L surfaces or if their adhesion is inhibited by repellent forces from the surfaces. As a result, the NT-SS316L surface displayed a bactericidal effect on Gram-negative *E. coli* cells, which ultimately reduced total adhesion of live cells on the NT-SS316L surfaces as compared to AR-SS316L in the CFU counts. The total adhered cell numbers, including live and dead cells, were similar on AR-SS316L and NT-SS316L surfaces after 30 min, while the NT-SS316L surfaces had greater number of dead cells (Figure 4). These

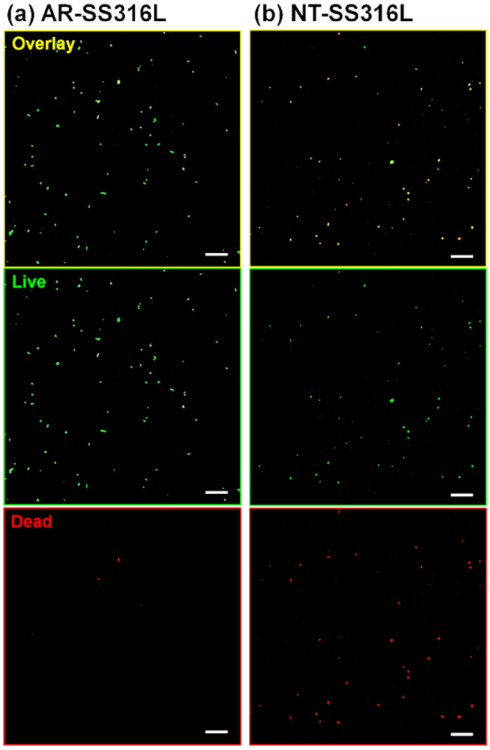

Figure 4. Representative fluorescent micrographs of *E. coli* cultured for 30 min on (a) AR-SS316L and (b) NT-SS316L surfaces (SYTO 9 and propidium iodide, respectively, stained live (green) and dead (red) bacterial cells). All scale bars are 30 μm.

results indicate that the bactericidal effect is more dominant than the antifouling effect. We hypothesize that the nanoprotrusive features of the NT-SS316L surfaces can induce mechanical stress on the membrane of adhered bacteria, resulting in cell death without the use of antibiotics or chemical coatings. The competition between cell membrane elasticity and the capillarity of the nanopores on SS316L surfaces can also enhance the deformation and stress of the bacterial membranes. This is the first report, to our knowledge, to demonstrate inhibition of both pathogenic Gram-positive and Gram-negative bacterial adhesion on SS316L surface with nanotextures and superior corrosion resistance.

To check applicability of the NT-SS316L in biomedicine, we further tested biocompatibility of the surfaces with mammalian cells. Fibroblast cells are connective tissue cells that play a crucial role in wound healing and numerous biomaterial applications and are one of the most common cells used in in vitro cytocompatibility tests of biomedical devices.[41,42] Given the general applications of SS316L materials for medical devices (i.e., surgical tools, implants, hospital pipes, and instruments) and food processing equipment, we selected NIH-3T3 murine fibroblasts as a model cell line to test in vitro cytotoxicity of the surfaces based on well-documented previous work.[41,42] We monitored the morphology of murine fibroblast cells (NIH-3T3) attached to NT-SS316L by SEM and conducted MTT assays for evaluation of the metabolic activity of NIH-3T3 cells, which corresponds to cytocompatibility of NT-SS316L surfaces. As shown in Figure 5a, SEM revealed that NIH-3T3 fibroblasts spread and elongated actively on the NT-SS316L surface with spindle-like and star-type shapes. This indicates successful attachment to the NT-SS316L surface. There was no difference in the fibroblast adhesion morphology on NT-SS316L compared to the AR-SS316L surface, which is a commercially available material for human implants (Figure 5b).[43] In addition, the metabolic activity of NIH-3T3 cells did not change on AR-SS316L and NT-SS316L surfaces for 24, 72, or 96 h of culture as compared to the PS culture dish control; this result indicates good cytocompatibility of NT-SS316L with mammalian cells (Figure 5c and Figure S5 in Supporting Information). All SS316L samples show cytocompatibility and active metabolism similar to what is observed on the polystyrene (PS) tissue culture dish. This result is in a good agreement with several already reported findings that nanotextured surfaces do not harm adhesion and proliferation of mammalian cells as compared with plain surfaces,[44,45] and in some cases slightly increase cell activity.[46]

We characterized surface structures, corrosion resistance, bacterial adhesion properties, and cytocompatibility of NT-SS316L surfaces created by electrochemical etching. The present study monitored adhesion of bacterial strains applicable to laboratory research and evaluated in vitro cytocompatibility on a short-term scale. Long-term in vivo studies are warranted in future work to evaluate practical applications of NT-SS316L surfaces. Nonetheless, these results contribute useful information about the effect of nanostructured surface on bacterial adhesion and suggest that the NT-SS316L materials developed in this study are promising candidates for biomedical applications based on the simple fabrication process and the materials' superior performance for corrosion resistance, bacterial adhesion/growth inhibition, and cytocompatibility.

DOI: 10.1021/acsbiomaterials.7b00544
ACS Biomater. Sci. Eng. 2018, 4, 90−97

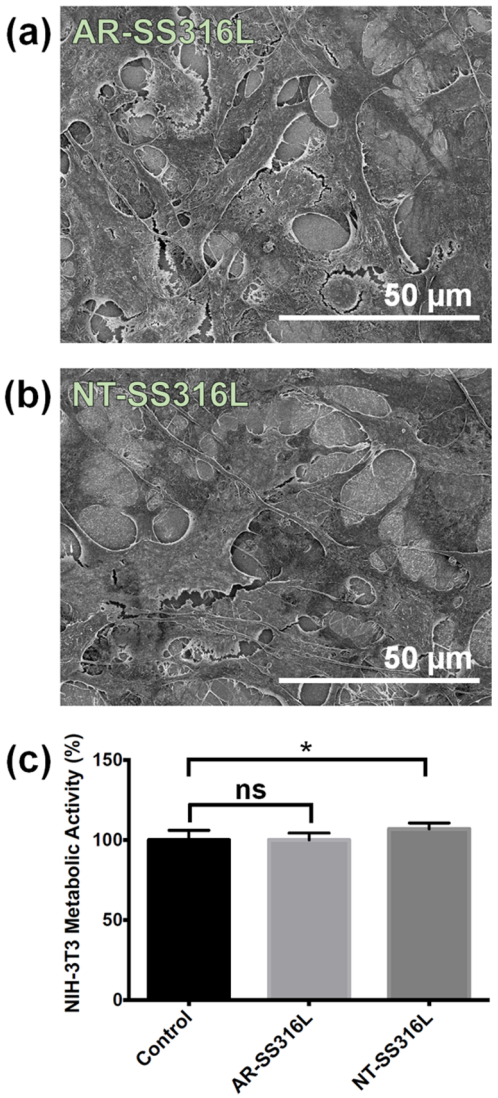

Figure 5. Cytocompatibility of the NT-SS316L surface. SEM images of NIH-3T3 cells cultured on (a) AR-SS316L and (b) NT-SS316L for 24 h. (c) Metabolic activity of NIH-3T3 fibroblast cells cultured on the AR- and NT-SS316L surfaces measured by MTT assay was compared to the control on a PS culture dish after 24 h. Data represent mean ± SEM ($N = 3$, $^*p < 0.05$).

CONCLUSION

We demonstrated the inhibition of both Gram-negative and Gram-positive bacterial adhesion and/or growth on a modified SS316L surface. Electrochemical etching was utilized to construct nanotextured SS316L surfaces comprised of 20−25 nm nanopores and nanoprotrusions, which effectively inhibit bacterial adhesion and are bactericidal while maintaining cytocompatibility toward mammalian cells. In addition, the NT-SS316L surfaces displayed Cr and Mo enrichment at the surface and improved corrosion resistance in physiological solution. Extensive utility of SS316L in the biomedical industry, inhibition of bacterial adhesion without the use of antibiotics or other transient coatings, biocompatibility to fibroblasts, formation of superior passive film for corrosion resistance, and process affordability and scalability make this approach of surface modification practically relevant.

ASSOCIATED CONTENT

Supporting Information

The Supporting Information is available free of charge on the ACS Publications website at DOI: 10.1021/acsbiomaterials.7b00544.

Surface height profiles of AR-SS316L and NT-SS316L obtained by AFM, Tafel fitting on a representative potentiodynamic polarization curve of SS316L sample in Hank's balanced salt solution, contact angles of deionized water droplets placed on AR-SS316L and NT-SS316L surfaces, SEM image of bacterial adhesion on micro-textured SS316L, and cytocompatibility of AR-SS316L and NT-SS316L surfaces after 72 and 96 h of culture of NIH-3T3 (PDF)

AUTHOR INFORMATION

Corresponding Authors

*E-mail: dennis.hess@chbe.gatech.edu.
*E-mail: julie.champion@chbe.gatech.edu.

ORCID

Victor Breedveld: 0000-0001-9108-7137
Julie A. Champion: 0000-0002-0260-9392

Author Contributions

⊥Y.J. and W.T.C. contributed equally to this work.

Notes

The authors declare no competing financial interest.

ACKNOWLEDGMENTS

This research was financially supported by M.T. Campagna. This work was performed in part at the Georgia Tech Institute for Electronics and Nanotechnology (IEN), a member of the National Nanotechnology Infrastructure Network, which is supported by the NSF. This work used core facilities of the Petit Institute of Bioengineering and Biosciences at Georgia Tech. C.T.J. and A.J.G. are funded by the National Institutes of Health (Grants F30 AR069472 and R01 AR062920).

REFERENCES

(1) Ribeiro, M.; Monteiro, F. J.; Ferraz, M. P. Infection of orthopedic implants with emphasis on bacterial adhesion process and techniques used in studying bacterial-material interactions. *Biomatter* **2012**, *2* (4), 176−194.
(2) Tuson, H. H.; Weibel, D. B. Bacteria-surface interactions. *Soft Matter* **2013**, *9* (17), 4368−4380.
(3) An, Y. H.; Friedman, R. J. Concise review of mechanisms of bacterial adhesion to biomaterial surfaces. *J. Biomed. Mater. Res.* **1998**, *43* (3), 338−348.
(4) Busscher, H. J.; Norde, W.; Sharma, P. K.; van der Mei, H. C. Interfacial re-arrangement in initial microbial adhesion to surfaces. *Curr. Opin. Colloid Interface Sci.* **2010**, *15* (6), 510−517.
(5) Knetsch, M. L. W.; Koole, L. H. New Strategies in the Development of Antimicrobial Coatings: The Example of Increasing Usage of Silver and Silver Nanoparticles. *Polymers* **2011**, *3* (1), 340−366.
(6) Tiller, J. C.; Liao, C.-J.; Lewis, K.; Klibanov, A. M. Designing surfaces that kill bacteria on contact. *Proc. Natl. Acad. Sci. U. S. A.* **2001**, *98* (11), 5981−5985.
(7) Qian, X.; Metallo, S. J.; Choi, I. S.; Wu, H.; Liang, M. N.; Whitesides, G. M. Arrays of Self-Assembled Monolayers for Studying Inhibition of Bacterial Adhesion. *Anal. Chem.* **2002**, *74* (8), 1805−1810.
(8) Yu, K.; Lo, J. C. Y.; Mei, Y.; Haney, E. F.; Siren, E.; Kalathottukaren, M. T.; Hancock, R. E. W.; Lange, D.;

DOI: 10.1021/acsbiomaterials.7b00544
ACS Biomater. Sci. Eng. 2018, 4, 90−97

Kizhakkedathu, J. N. Toward Infection-Resistant Surfaces: Achieving High Antimicrobial Peptide Potency by Modulating the Functionality of Polymer Brush and Peptide. *ACS Appl. Mater. Interfaces* **2015**, *7* (51), 28591−28605.
(9) Cheng, G.; Zhang, Z.; Chen, S.; Bryers, J. D.; Jiang, S. Inhibition of bacterial adhesion and biofilm formation on zwitterionic surfaces. *Biomaterials* **2007**, *28* (29), 4192−4199.
(10) Kenawy, E.-R.; Worley, S. D.; Broughton, R. The Chemistry and Applications of Antimicrobial Polymers: A State-of-the-Art Review. *Biomacromolecules* **2007**, *8* (5), 1359−1384.
(11) Banerjee, I.; Pangule, R. C.; Kane, R. S. Antifouling Coatings: Recent Developments in the Design of Surfaces That Prevent Fouling by Proteins, Bacteria, and Marine Organisms. *Adv. Mater.* **2011**, *23* (6), 690−718.
(12) Wu, S. M.; Zuber, F.; Brugger, J.; Maniura-Weber, K.; Ren, Q. Antibacterial Au nanostructured surfaces. *Nanoscale* **2016**, *8* (5), 2620−2625.
(13) Jahed, Z.; Lin, P.; Seo, B. B.; Verma, M. S.; Gu, F. X.; Tsui, T. Y.; Mofrad, M. R. K. Responses of Staphylococcus aureus bacterial cells to nanocrystalline nickel nanostructures. *Biomaterials* **2014**, *35* (14), 4249−4254.
(14) Liu, L. T.; Ercan, B.; Sun, L. L.; Ziemer, K. S.; Webster, T. J. Understanding the Role of Polymer Surface Nanoscale Topography on Inhibiting Bacteria Adhesion and Growth. *ACS Biomater. Sci. Eng.* **2016**, *2* (1), 122−130.
(15) Kim, S.; Jung, U. T.; Kim, S. K.; Lee, J. H.; Choi, H. S.; Kim, C. S.; Jeong, M. Y. Nanostructured Multifunctional Surface with Antireflective and Antimicrobial Characteristics. *ACS Appl. Mater. Interfaces* **2015**, *7* (1), 326−331.
(16) Feng, G.; Cheng, Y.; Wang, S.-Y.; Hsu, L. C.; Feliz, Y.; Borca-Tasciuc, D. A.; Worobo, R. W.; Moraru, C. I. Alumina surfaces with nanoscale topography reduce attachment and biofilm formation by Escherichia coli and Listeria spp. *Biofouling* **2014**, *30* (10), 1253−1268.
(17) Feng, G.; Cheng, Y.; Wang, S.-Y.; Borca-Tasciuc, D. A.; Worobo, R. W.; Moraru, C. I. Bacterial attachment and biofilm formation on surfaces are reduced by small-diameter nanoscale pores: how small is small enough? *NPJ. Biofilms Microbiomes* **2015**, *1*, 15022.
(18) Ivanova, E. P.; Hasan, J.; Webb, H. K.; Gervinskas, G.; Juodkazis, S.; Truong, V. K.; Wu, A. H. F.; Lamb, R. N.; Baulin, V. A.; Watson, G. S.; Watson, J. A.; Mainwaring, D. E.; Crawford, R. J. Bactericidal activity of black silicon. *Nat. Commun.* **2013**, *4*, 2838.
(19) Dewidar, M. M.; Khalil, K. A.; Lim, J. K. Processing and mechanical properties of porous 316L stainless steel for biomedical applications. *Trans. Nonferrous Met. Soc. China* **2007**, *17* (3), 468−473.
(20) Bagherifard, S.; Hickey, D. J.; de Luca, A. C.; Malheiro, V. N.; Markaki, A. E.; Guagliano, M.; Webster, T. J. The influence of nanostructured features on bacterial adhesion and bone cell functions on severely shot peened 316L stainless steel. *Biomaterials* **2015**, *73*, 185−197.
(21) Kathiresan, S.; Mohan, B. In-vitro bacterial adhesion study on stainless steel 316L subjected to magneto rheological abrasive flow finishing. *Biomed. Res. (Aligarh, India)* **2017**, *28* (7), 3169−3175.
(22) Singh, A. V.; Vyas, V.; Patil, R.; Sharma, V.; Scopelliti, P. E.; Bongiorno, G.; Podesta, A.; Lenardi, C.; Gade, W. N.; Milani, P. Quantitative Characterization of the Influence of the Nanoscale Morphology of Nanostructured Surfaces on Bacterial Adhesion and Biofilm Formation. *PLoS One* **2011**, *6* (9), e25029.
(23) Slama, T. G. Gram-negative antibiotic resistance: there is a price to pay. *Crit. Care* **2008**, *12*, 4.
(24) Perfeito, L.; Fernandes, L.; Mota, C.; Gordo, I. Adaptive mutations in bacteria: High rate and small effects. *Science* **2007**, *317* (5839), 813−815.
(25) Cremet, L.; Broquet, A.; Brulin, B.; Jacqueline, C.; Dauvergne, S.; Brion, R.; Asehnoune, K.; Corvec, S.; Heymann, D.; Caroff, N. Pathogenic potential of *Escherichia coli* clinical strains from orthopedic implant infections towards human osteoblastic cells. *Pathog. Dis.* **2015**, *73* (8), ftv065.
(26) Choi, W. T.; Oh, K.; Singh, P. M.; Breedveld, V.; Hess, D. W. Wettability control of stainless steel surfaces via evolution of intrinsic grain structures. *J. Mater. Sci.* **2016**, *51* (11), 5196−5206.
(27) Choi, W. T.; Oh, K.; Singh, P. M.; Breedveld, V.; Hess, D. W. Hydrophobicity and Improved Localized Corrosion Resistance of Grain Boundary Etched Stainless Steel in Chloride-containing Environment. *J. Electrochem. Soc.* **2017**, *164* (2), C61−C65.
(28) Khan, M. F.; Luong, N.; Kurian, J.; Brook, M. A. Superwetting comonomers reduce adhesion of *E. coli* BL21. *Chem. Commun.* **2017**, *53* (21), 3050−3053.
(29) Beenken, K. E.; Blevins, J. S.; Smeltzer, M. S. Mutation of sarA in *Staphylococcus aureus* limits biofilm formation. *Infect. Immun.* **2003**, *71* (7), 4206−4211.
(30) Sanders, E. R. Aseptic Laboratory Techniques: Plating Methods. *J. Visualized Exp.* **2012**, *63*, 3064.
(31) Medilanski, E.; Kaufmann, K.; Wick, L. Y.; Wanner, O.; Harms, H. Influence of the surface topography of stainless steel on bacterial adhesion. *Biofouling* **2002**, *18* (3), 193−203.
(32) Riedewald, F. Bacterial Adhesion to Surfaces: The Influence of Surface Roughness. *PDA J. Pharm. Sci. Technol.* **2005**, *60*, 164−171.
(33) Ivanova, E. P.; Hasan, J.; Webb, H. K.; Truong, V. K.; Watson, G. S.; Watson, J. A.; Baulin, V. A.; Pogodin, S.; Wang, J. Y.; Tobin, M. J.; Lobbe, C.; Crawford, R. J. Natural Bactericidal Surfaces: Mechanical Rupture of *Pseudomonas aeruginosa* Cells by Cicada Wings. *Small* **2012**, *8* (16), 2489−2494.
(34) Sivakumar, M.; Kumar Dhanadurai, K. S.; Rajeswari, S.; Thulasiraman, V. Failures in stainless steel orthopaedic implant devices: A survey. *J. Mater. Sci. Lett.* **1995**, *14* (5), 351−354.
(35) Beddoes, J.; Bucci, K. The influence of surface condition on the localized corrosion of 316L stainless steel orthopaedic implants. *J. Mater. Sci.: Mater. Med.* **1999**, *10* (7), 389−394.
(36) Shibata, T.; Takeyama, T. Stochastic Theory of Pitting Corrosion. *Corrosion* **1977**, *33* (7), 243−251.
(37) Shibata, T. Stochastic studies of passivity breakdown. *Corros. Sci.* **1990**, *31*, 413−423.
(38) Jones, D. A. *Principles and Prevention of Corrosion*, 2nd ed.; Prentice Hall: Upper Saddle River, NJ, 1996.
(39) Hultquist, G.; Leygraf, C. Surface Composition of a Type 316 Stainless Steel Related to Initiation of Crevice Corrosion. *Corrosion* **1980**, *36* (3), 126−129.
(40) Rizzello, L.; Galeone, A.; Vecchio, G.; Brunetti, V.; Sabella, S.; Pompa, P. P. Molecular response of *Escherichia coli* adhering onto nanoscale topography. *Nanoscale Res. Lett.* **2012**, *7* (1), 575.
(41) McDaniel, C.; Gladkovskaya, O.; Flanagan, A.; Rochev, Y.; O'Connor, G. M. In vitro study on the response of RAW264.7 and MS-5 fibroblast cells on laser-induced periodic surface structures for stainless steel alloys. *RSC Adv.* **2015**, *5* (53), 42548−42558.
(42) Groessner-Schreiber, B.; Neubert, A.; Muller, W. D.; Hopp, M.; Griepentrog, M.; Lange, K. P. Fibroblast growth on surface-modified dental implants: An in vitro study. *J. Biomed. Mater. Res., Part A* **2003**, *64a* (4), 591−599.
(43) Ionescu, R.; Mardare, M.; Dorobantu, A.; Vermesan, S.; Marinescu, E.; Saban, R.; Antoniac, I.; Ciocan, D. N.; Ceausu, M. Correlation Between Materials, Design and Clinical Issues in the Case of Associated Use of Different Stainless Steels as Implant Materials. *Key Eng. Mater.* **2013**, *583*, 41−44.
(44) Xavier, S. P.; Carvalho, P. S. P.; Beloti, M. M.; Rosa, A. L. Response of rat bone marrow cells to commercially pure titanium submitted to different surface treatments. *J. Dent.* **2003**, *31* (3), 173−180.
(45) Izquierdo-Barba, I.; Garcia-Martin, J. M.; Alvarez, R.; Palmero, A.; Esteban, J.; Perez-Jorge, C.; Arcos, D.; Vallet-Regi, M. Nano-columnar coatings with selective behavior towards osteoblast and *Staphylococcus aureus* proliferation. *Acta Biomater.* **2015**, *15*, 20−28.
(46) Webster, T. J.; Ejiofor, J. U. Increased osteoblast adhesion on nanophase metals: Ti, Ti6Al4V, and CoCrMo. *Biomaterials* **2004**, *25* (19), 4731−4739.

DOI: 10.1021/acsbiomaterials.7b00544
ACS Biomater. Sci. Eng. 2018, 4, 90−97